Volume 6
Number 3
March 2021
Pages 357–574

# Reaction Chemistry & Engineering

Linking fundamental chemistry and engineering to create scalable, efficient processes

rsc.li/reaction-engineering

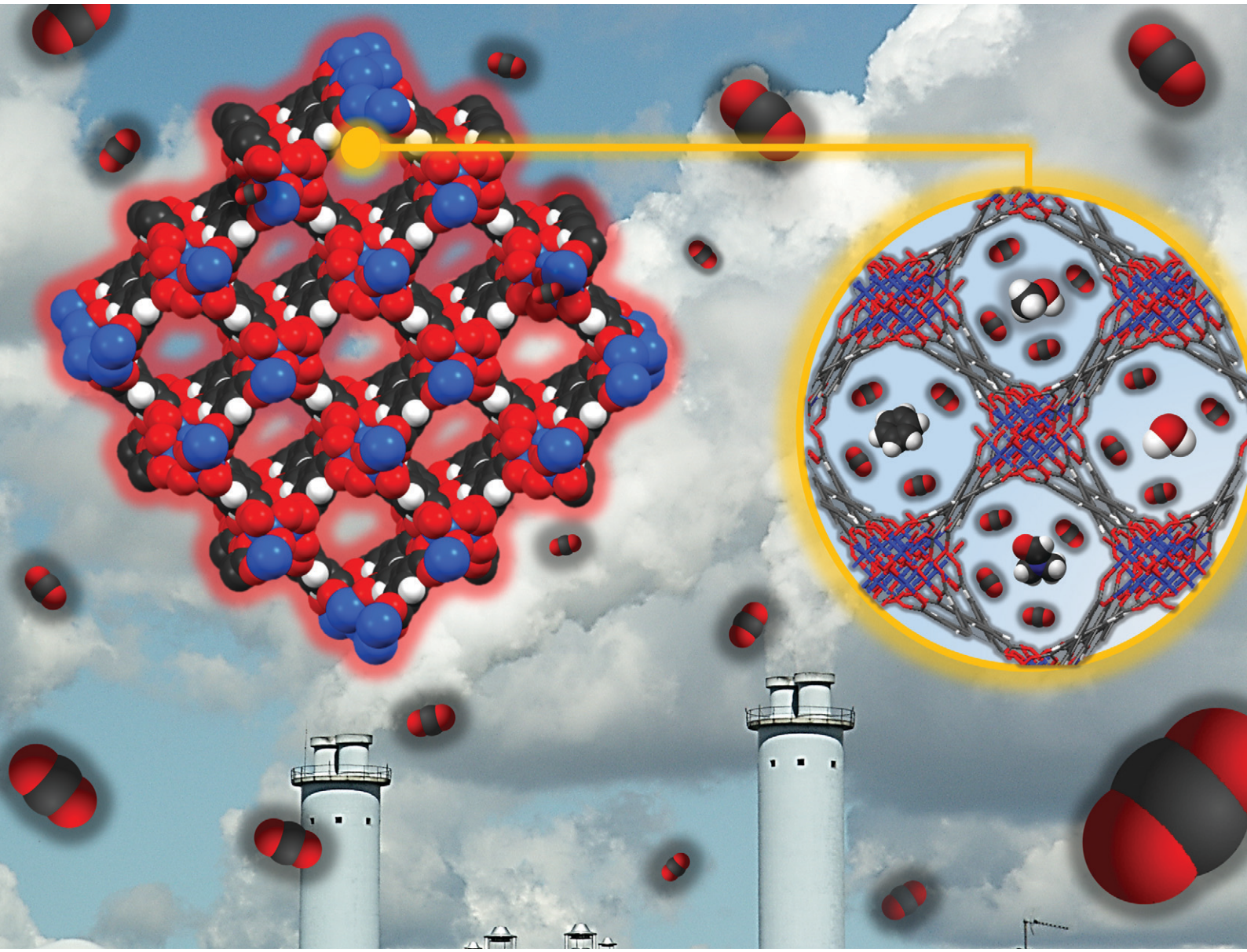

ISSN 2058-9883

ROYAL SOCIETY OF CHEMISTRY

**MINIREVIEW**

Eduardo González-Zamora, Ilich A. Ibarra *et al.*
$CO_2$ capture enhancement in MOFs *via* the confinement of molecules

Reaction Chemistry & Engineering

ROYAL SOCIETY OF CHEMISTRY

MINI REVIEW

View Article Online
View Journal | View Issue



Cite this: *React. Chem. Eng.*, 2021, **6**, 441

# $CO_2$ capture enhancement in MOFs *via* the confinement of molecules

Vanesa del C. Cotlame-Salinas,†[a] Alfredo López-Olvera,†[b] Alejandro Islas-Jácome,[a] Eduardo González-Zamora *[a] and Ilich A. Ibarra *[b]

Received 23rd October 2020,
Accepted 4th January 2021

DOI: 10.1039/d0re00410c

rsc.li/reaction-engineering



Metal–organic frameworks (MOFs) have become the most promising molecular sponges to capture gases contributing to the greenhouse effect, *e.g.* $CO_2$, due to various desirable features such as tuneable pore shapes, sizes and functionalities, a great surface area, resistance to harsh conditions (wide ranges of pH, temperatures, humidity, *etc.*), ease of their preparation, and in most cases, a high degree of recovery. Thus, despite many MOFs adsorbing extensive amounts of $CO_2$ in their pristine form, it has been demonstrated that their uptake capability can be considerably enhanced when they are post-synthetically modified by the confinement of molecules with different polarities, as a result of new physical–chemical interactions between the pre-confined species and the $CO_2$ molecules within their cavities, for example, *via* the bottleneck effect, H-bonds and/or even π–π stacking interactions. Thus, this review covers selected studies, mainly from the last five years, highlighting the most significant advances on the $CO_2$ enhanced uptake performance of selected MOFs with pre-adsorbed polar (water, alcohols, and amines) and non-polar (toluene and benzene) molecules, as well as some interesting findings from robust computational calculations behind understanding the nature of such host–guest interactions, with the latter one being a practical and useful tool in the research field.

## 1. Introduction

The impact of climate change on human health is one of the most important concerns in contemporary society. This issue not only causes direct damage to the world (severe storms, floods, prolonged heatwaves and droughts)[1] but also can indirectly damage human health by deteriorating the environment and changing the balance of different ecosystems, which develops many diseases while hindering their prevention and treatment.[2] Global warming is mainly caused by a group of gases better known as greenhouse gases, such as: methane ($CH_4$); nitrous oxides ($NO_X$), fluorinated gases and carbon dioxide ($CO_2$).[3] In fact, the increase of the levels of $CO_2$ emissions in the atmosphere, due to the excessive consumption of fossil fuels (coal, natural gas and oil),[4] has become a global environmental concern.[5] According to the EPA's report,[6] in 2018, the total $CO_2$ emission was 6667 million metric tons (81% of all greenhouse gases), which comes mostly from anthropogenic sources. It is known that $CO_2$ is removed from the atmosphere by different natural processes. Unfortunately, the large amounts of $CO_2$ released into the atmosphere exceed natural remediation processes. Thus, the design and immediate implementation of new recovery systems is imperative.

Over the years, numerous research studies and technologies have been implemented to capture $CO_2$ from industry emissions and store it through chemical/physical strategies.[7] One of the main techniques applied in $CO_2$ sequestration is the use of alkanolamines in aqueous solution (by a chemisorption process), performing as a Lewis base.[8] Nevertheless, such an absorption method has shown many drawbacks such as: deterioration of pipelines, by-product formation and high recovery costs.[9] Therefore, it is essential to migrate towards more effective ways to decrease $CO_2$ waste. Comparatively, physical adsorption with porous materials such as adsorbents is extensively used for $CO_2$ capture due to environmental benefits and economic viability. Different porous solid adsorbent materials, such as zeolites, activated carbons and metal oxides, have been design for $CO_2$ adsorption.[10] Relevant features such as high selectivity and adsorption capacity, recyclability, good thermal and chemical stability, and fast kinetics, along with profitable costs, are necessary for a good $CO_2$ adsorbent material.

[a] *Departamento de Química, Universidad Autónoma Metropolitana-Iztapalapa, San Rafael Atlixco 186, Col. Vicentina, C.P. 09340, Iztapalapa, Ciudad de México, Mexico. E-mail: egz@xanum.uam.mx*
[b] *Laboratorio de Fisicoquímica y Reactividad de Superficies, Instituto de Investigaciones en Materiales, Universidad Nacional Autónoma de México, Circuito Exterior S/N, Ciudad Universitaria, Coyoacán, Ciudad de México, C.P. 04510, Mexico. E-mail: argel@unam.mx*
† These authors contributed equally to this work.

Undoubtedly, zeolites are the most widely studied adsorbents for $CO_2$ capture.[11] These micro–mesoporous solids (pore size between 0–2 and 2–50 nm, respectively) are constructed from aluminosilicates with different polyvalent cations, in a tetrahedral array. Even though zeolites have been a great support in the development of the science of modern porous materials,[12] some of these classical porous solids have shown critical constraints for $CO_2$ adsorption (*e.g.*, a high hydrophilic character and high dehydration temperature), meaning their exclusion for $CO_2$ removal under humid conditions.[13]

In the last decade, several adsorbent materials have been developed, including ionic liquids (ILs), porous organic polymers (POPs), and metal–organic materials (MOMs), among others.[14] Metal–organic frameworks (MOFs), also known as porous coordination polymers (PCPs), are a subclass of MOMs that have shown an exceptional adsorbent ability comparable to other porous materials. MOFs are a relatively new type of crystalline micro–mesoporous solid material constructed from strong interactions (coordination bonds) between metal clusters and organic ligands (classically carboxylic acids or azo compounds), generating robust arrays in 1, 2 or 3 dimensions.

Along with a diverse selection of inorganic metal nodes and organic ligands, and different synthetic methodologies, these materials have demonstrated tuneable physical/chemical properties, highlighting ultrahigh porosity, a large surface area and high thermal/chemical stability. These features clearly postulate MOFs as promising materials for $CO_2$ capture.[15] The combustion of fossils fuels, in many industrial processes, releases flue streams which include gases such as $CO_2$, CO, $CH_4$, $N_2$ and water vapour (5 to 7 wt%).[16] One of the main disadvantages of a large majority of MOF materials is their low stability toward $H_2O$. Furthermore, $H_2O$ molecules can, in some cases, disrupt the coordination bonds between the organic ligands and metal nodes, followed by partial or total fragmentation of the MOF structure. For instance, MOFs containing Zn–COOH bonds, such as DMOF-1, DMOF-1-$NH_2$ and UMCM-1, suffer from a complete loss of crystallinity under exposure to water.[17] Thus, a fundamental prerequisite for MOF materials is water stability which is key to $CO_2$ capture under humid conditions.[18]

In addition, the ideal adsorbent for $CO_2$ capture should show two main characteristics: a high $CO_2$ adsorption capacity at a low loading pressure between 0.05 to 0.15 bar;[19] and a good balance with a reversible adsorption/desorption process with a moderate heat of adsorption of 30–60 kJ $mol^{-1}$ (cycles).[20] Therefore, to achieve these points in the field of MOF materials, it is necessary to use the modulation of their chemical–physical properties, by a new process or post-synthetic modification (PSM). According to several research groups,[21] there are three foremost approaches to improve the $CO_2$ capture in MOFs based on the increment of the strength of the interaction between $CO_2$ and MOFs (primarily *via* their functional groups). These approaches are: (i) direct modification of organic linkers by insertion of polar functional groups (–$NH_2$, –OH, –COOH, –CN, –SH, and –$NO_2$ ).[22] An improvement in the $CO_2$ capture has been observed in different examples, such as amine functionalised CAU-1.[23] (ii) Generation of metal uncoordinated sites, also known as open metal sites (OMSs).[24] These OMSs are generated when a MOF is treated by a thermal or vacuum process to remove terminal labile linkers (usually synthetic solvents) binding to metal clusters. Thus, the quadrupole of $CO_2$ molecules can interact with metal Lewis acid sites. (iii) The confinement of molecules within MOFs such as water, alcohols, and amines and even the use of corrosive gases (*e.g.*, $H_2S$) have demonstrated an improvement in the $CO_2$ capture.[21,25] This review is focused on the last approach and determinant topics as the nature of solvents and their polarity will be comprehensibly discussed in the following sections.

In this context, it is known that the affinity of MOFs for polar molecules can increase for MOFs based on inorganic cluster chains with $\mu_x$-OH bridging groups.[25,26] This architecture can form hydrogen bonds between such bridging ($\mu_x$-OH) groups and confined molecules.[27] In general, this functionalisation can enhance the $CO_2$ adsorption properties of MOFs by confining small amounts of polar and non-polar molecules.

In the last decade, the main use of small alcohols (*i.e.*, methanol and ethanol) as working fluids in MOFs for heat-pump chillers have increased considerably.[27,28] Additionally, other uses of these polar molecules in MOFs have gained attention for the improvement of the $CO_2$ adsorption performance (*via* the pre-confinement of alcohols).[21] Following the strategy of confining small quantities of water and alcohols, new research has been carried out on the confinement of different polar molecules (amines) and non-polar molecules (hydrocarbons) for the enhancement of $CO_2$ uptake.

Major breakthroughs by the confinement of small amounts of molecules have been achieved in the last 4 years. Therefore, this review aims to give a broad overview grouping these advances, taking water confinement as the starting point, and the use of other molecules (polar and non-polar), to explain the fundamental molecular interactions responsible for the enhancement of the $CO_2$ capture in functionalised MOFs. Finally, with this review we try to encourage more research groups to explore and extend the knowledge on the effects of confining molecules within MOF materials.

## 2. Water pre-confinement

Despite the fact that the presence of water has a detrimental effect in gas adsorption processes of several MOFs due to structural collapse or a reduction in the amount of adsorption sites, some research groups have focused on the use of water as a fundamental tool in the enhancement of $CO_2$ adsorption under closely related industrial conditions (*vide supra*). In this section, we provide a brief discussion about some studies that we consider as a benchmark in the

 

development of pre-confinement of water to improve the $CO_2$ adsorption properties of MOF materials. One of the first steps toward understanding the influence of pre-confinement of water inside of MOFs was published in 2009 by Snurr *et al.*[28] As already recompiled in other reviews,[25,26b] this work shows how small amounts of water (4 wt% and 8 wt%) improve the $CO_2$ capture on a MOF based on Cu(II) with OMS called HKUST-1. This early study demonstrated that the confinement of water inside MOFs could be a new and better alternative for capturing $CO_2$ than using other classical materials (zeolites and activated carbons) that have shown several disadvantages in $CO_2$ removal under humid conditions. A few years later, Llewellyn and co-workers[29] reported an interesting systematic study, where they explored the effect of water on $CO_2$ uptake and the variations in the adsorption enthalpy in two microporous and one mesoporous MOFs: HKUST-1, UiO-66 (Zr) and MIL-100 (Fe), respectively, under post-combustion conditions (0.2 bar of $CO_2$ pressure and 298 K). This work can be considered as the cornerstone in the pre-confinement of water in MOF materials, due to the outstanding improvement of the $CO_2$ adsorption under humid conditions showed for the mesoporous MOF (MIL-100(Fe)) (Table 1), and the intriguing $CO_2$ adsorption mechanism that was suggested by the authors. Taking into account the significant advances made by Llewellyn and co-workers, our research group decided to delve into water confinement in microporous MOF materials. Thus, we developed several studies based on a set of microporous water-stable MOF materials decorated with hydroxo bridge groups ($\mu_x$-OH) such as MFM-300 (In and

**Table 1** Summary of MOF materials reported in the literature for $CO_2$ capture under wet conditions

| MOF material | Surface area BET [$m^2\ g^{-1}$] | Press. [bar] | Temp [K] | $CO_2$ adsorption under dry conditions [mmol $g^{-1}$] | Amount of water pre-adsorbed | $CO_2$ adsorption under wet conditions [mmol $g^{-1}$] | Ref. |
|---|---|---|---|---|---|---|---|
| HKUST-1 | 1387 | 1 | 298 | 4.88[a] | 4 wt% | 8.63[a] | 38 |
| HKUST-1-pellet | 921 | 1 | 298 | 2.90[a] | 1.8 wt%[a] | 3.25[a] | 39 |
| Mg-MOF-74 | 1495 | 0.167 | 298 | 4.91[a] | 9% RH | 1.63[a] | 40 |
| | | | | | 36% RH | 1.22[a] | |
| | | | | | 70% RH | 0.77[a] | |
| Co-MOF-74 | 1080 | 0.167 | 298 | 2.78[a] | 70% RH | 2.37[a] | 39 |
| Co-MOF-74 | 1105 | 1 | 298 | 6.14 | 15.6 wt% | 4.46 | 41 |
| Zn-MOF-74 | 816 | 0.167 | 298 | 1.51[a] | 70% RH | 0.32[a] | 39 |
| Ni-MOF-74 | 1070 | 0.167 | 298 | 2.62[a] | 70% RH | 1.59[a] | 38 |
| NiMOF-74-pellet | 639 | 1 | 298 | 6.68[a] | 1.8 wt%[a] | 6.45[a] | 38 |
| MIL-100(Cr) | 1790 | 1 | 303 | 1.42 | 5.83 wt[a] | 0.71 | 42 |
| MIL-100(Fe) | 2006 | 0.2 | 298 | 0.50 | 1 wt%[a] | 0.59 | 29 |
| | | | | | 3 wt%[a] | 0.54 | |
| | | | | | 4.8 wt%[a] | 1.52 | |
| | | | | | 55 wt%[a] | 2.47 | |
| UiO-66(Zr) | 1179 | 0.2 | 298 | 0.61 | 1 wt%[a] | 0.77 | 29 |
| | | | | | 2 wt%[a] | 0.75 | |
| | | | | | 4 wt%[a] | 0.75 | |
| | | | | | 18 wt%[a] | 0.79 | |
| MIL-101(Cr) | 3314 | 0.1 | 298 | 0.50 | 20% RH | 0.48 | 43 |
| $[Cu(PF_6)_2(bpp)_2]_n$ | — | 10 | 298 | 1.31 | 17% RH | 1.34 | 44 |
| ZIF-68 | — | 0.1 | 298 | 0.029 | 50 wt%[a] | 0.029 | 45 |
| PCN-250($Fe_3$) | 1470 | 0.15 | 298 | 1.18 | 50% RH | 1.82 | 38 |
| | | | | | 90% RH | 1.52 | |
| PCN-250($Fe_2Co$) | 1653 | 0.15 | 298 | 1.32 | 50% RH | 2.23 | 37 |
| | | | | | 90% RH | 2.27 | |
| MFM-300(In) | 1060 | K. C | 298 | 1.23 | 30% RH | 2.5 | 30 |
| MFM-300(Sc) | 1356 | K. C | 303 | 0.93 | 1.7 wt%[a] | 1.8 | 31 |
| | | | | | 2.2 wt%[a] | 2.31 | |
| NOTT-401 | 1504 | K. C | 303 | 0.27 | 1.1% wt[a] | 0.88 | 32 |
| | | | | | 3.0 wt%[a.] | 0.43 | |
| | | | | | 4.2 wt%[a] | 0.09 | |
| MIL-53(Al) | 1096 | K. C | 303 | 0.79 | 1.5 wt%[a] | 1.18 | 33 |
| MIL-53(Al)-TDC | 1443 | K. C | 303 | 1.13 | 0.60 wt% | 1.47 | 34 |
| CAU-10 | 615 | K. C | 303 | 1.22 | 0.55 wt% | 1.65 | 35 |
| Mg-CUK-1 | 600 | K. C | 303 | 1.04 | 0.2 wt% | 1.12 | 36 |
| | | | | | 0.5 wt% | 1.20 | |
| | | | | | 0.8 wt% | 1.92 | |
| | | | | | 0.9 wt% | 1.94 | |
| | | | | | 1.4 wt% | 1.89 | |
| | | | | | 1.7 wt% | 1.82 | |
| Fe(pz)[$Pt(CN)_4$] | 431 | K. C | 298 | 2.11 | 11.7% | 0.6 | 46 |

[a] Values calculated from the experimental dates (some have been converted to wt% from the originally reported units). K. C: kinetic conditions.

Sc),[30,31] NOTT-401,[32] MIL-53(Al) (BDC and TDC),[33,34] CAU-10 (ref. 35) and Mg-CUK-1,[36] working in a minimal range of quantity of confined water from 0.5 to 4 wt% on average (Table 1). For example, it was demonstrated that although CAU-10 does not have a considerable surface area, compared to other representative MOFs,[37] this porous solid can achieve a 1.3-fold $CO_2$ enhancement (*i.e.*, from 1.2 to 1.65 under dry and wet conditions respectively) only using 0.55 wt% water (Table 1). Besides, CAU-10 shows an excellent cyclability performance, being stable up to 5 cycles with minimal changes in its adsorption properties. Mg-CUK-1 (ref. 36) demonstrated an outstanding performance reaching a maximum for the $CO_2$ capture of almost 1.9-fold with 0.9 wt% of preconfined water (Table 1). Overall, such enhancement showed for these materials is associated with the polar environment inside the pores which is provided by the hydroxo bridging groups (either $\mu_3$-OH or -$\mu_2$-OH), which form hydrogen bonds with water molecules at low-charge, and the water molecules fixed in the pores can accommodate very efficiently $CO_2$ molecules by weak interactions. The possible adsorption mechanism of $CO_2$ under humid conditions is supported by computational calculations. Thus, these findings are an interesting guideline to evaluate other molecules for a higher $CO_2$ capture.

Recently,[38] in 2018, Chen and Li reported two water-stable microporous MOF materials: PCN-250 ($Fe_3$) and PCN-250 ($Fe_2Co$), which were evaluated using 50 and 90% RH at 298 K and dynamic adsorption conditions. These framework materials were constructed from $Fe_3(\mu_3\text{-O})(CH_3COO)_6$ or $Fe_2Co(\mu_3\text{-O})(CH_3COO)_6$ metal clusters, respectively, and the $H_4$ABTC organic linker ($H_4$ABTC = 3,3′,5,5′-azobenzenetetracarboxylic acid). Both materials showed substantial enhancement in the $CO_2$ uptake under humid conditions (*i.e.*, $CO_2$ captures achieved at 50% RH were 1.82 and 2.23 mmol $g^{-1}$while those at 90% RH were 1.52 and 2.27 mmol $g^{-1}$ for PCN-250 ($Fe_3$) and PCN-250 ($Fe_2Co$), respectively). The amount of $CO_2$ adsorbed for both materials under dry conditions was 1.18 and 1.23 mmol $g^{-1}$, respectively. The authors attributed this improvement to the influence of the oxo bridged groups ($\mu_3$-O) within the pore environment for both frameworks in the presence of water, such functional group acts as a clamp-like mechanism. Finally, the authors mentioned that both microporous solids showed a remarkable cyclability performance (up to 10 cycles) without showing any change in their crystalline structure.

## 3. Alcohol and amine molecule confinement for $CO_2$ capture

Following the previous approach, it was interesting to explore the effect on $CO_2$ adsorption in MOFs when other polar solvents were confined in their channels. Thus, a series of studies have been reported since 2016, concerning the confinement of different alcohols (MeOH, EtOH, 1-PrOH and 2-PrOH) in MOF materials (MFM-300(In),[47–50] HKUST-1,[51] MIL-53(Al)[52] and MIL-53(Al)-TDC).[34]

The initial study involved the MOF material labeled MFM-300(In) (also known as InOF-1) and confined ethanol.[47] MFM-300(In) is a microporous material constructed from binuclear [$In_2(\mu_2$-OH)] building blocks linked by $BPTC^{4-}$ ligands ($H_4$BPTC = biphenyl-3,3′,5,5′-tetracarboxylic acid), forming a 3D structure with channel dimensions of 7.5 Å (Fig. 1).

Kinetic and static $CO_2$ adsorption studies of a pre-loaded (confined) MFM-300(In) sample with 2.63 wt% ethanol were carried out. The results showed an enhancement in the $CO_2$ adsorption capabilities in both systems, reaching a maximum $CO_2$ capture of 2.7-fold under kinetic conditions (3.21 mmol $g^{-1}$) and 3.6-fold (3.11 mmol $g^{-1}$) under static conditions, at 1 bar of $CO_2$ pressure, compared to dry adsorption measurements (1.19 mmol $g^{-1}$ and 0.86 mmol $g^{-1}$, respectively). This behavior was attributed to the presence of hydrogen bonds between hydroxo bridging groups (μ-OH) and EtOH molecules that substantially diminished the dimensions of the channels and changed the shape of the pores, producing a partial obstruction. Consequently, when a flow of $CO_2$ molecules crosses the channels, the obstructed pores reduce the self-diffusion coefficient of $CO_2$ molecules. This effect was designated as the "bottleneck effect". Fig. 2 shows the pore reduction of MFM-300(In) as a function of preconfined ethanol. An amount of 2.63 wt% ethanol represents approximately 1.35 molecules of ethanol per unit cell, and the distribution of the confined molecules creates "bottlenecks" separated in sections of 37 Å, forcing the $CO_2$ molecules to stay longer around the bottleneck due to steric effects. Thus, $CO_2$ molecules can be accommodated more efficiently inside the channels. Recently, in 2020, it was reported that such a bottleneck effect also occurs in Mg-CUK-1 (ref. 53) when water molecules were confined inside the pores and a $CO_2$ uptake enhancement of 1.8-fold was achieved. This effect was successfully demonstrated by PXRD with Le Bail methodology refinements.

Later, some studies related to the confinement of alcohols with different kinetic diameters were presented. Thus, the confinement of methanol within MFM-300(In) was reported

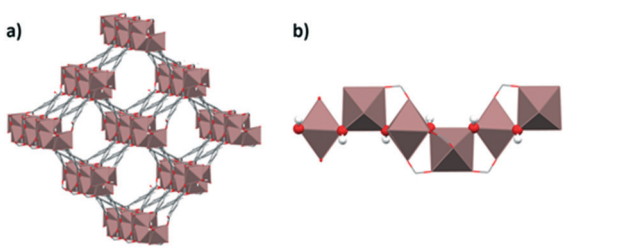


Fig. 1 a) MFM-300(In) 3D structural view along the crystallographic axis *c*, showing the pore opening. b) Inorganic oxo-cluster chain with In(III) in octahedral coordination geometry, showing the position of the $\mu_2$-OH bridge groups.

 

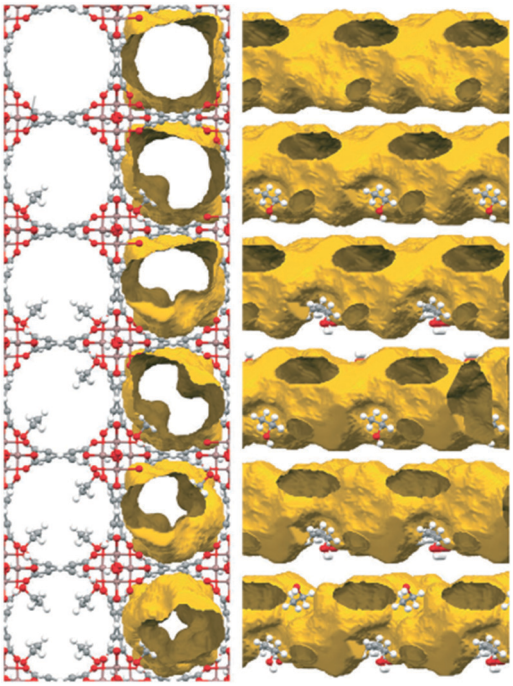

Fig. 2 Crystal structure of MFM-300(In) and the effect of the amount of ethanol confined in the pores *via* the formation of a hydrogen bond to the $In_2(\mu_2$-OH) hydroxo groups on the pore diameter and shape. View along the crystallographic 001 direction with and without the channel surface (left) and along the 110-direction rotated additionally by 35° around 010 (right) to demonstrate the change from an almost cylindrical shape to a helicoidal shape (reproduced from ref. 47 with permission from The Royal Society of Chemistry).

in 2017.[48] The material loaded with 2 wt% MeOH showed an interesting $CO_2$ uptake enhancement. Kinetic and static $CO_2$ isotherms exhibited a 1.3-fold and 4.88-fold increase in the $CO_2$ adsorption capacity, respectively (from 1.19 mmol $g^{-1}$ to 1.56 mmol $g^{-1}$ under kinetic conditions and from 0.26 mmol $g^{-1}$ to 1.27 mmol $g^{-1}$ under static conditions) (Fig. 3). This improvement was corroborated by computational Monte Carlo (MC) calculations, which illustrated the preferential adsorption sites for the MeOH molecules near the $\mu_2$-OH groups, tending to form lumps, and hence reducing the pore dimensions (Fig. 4). This explanation supported the

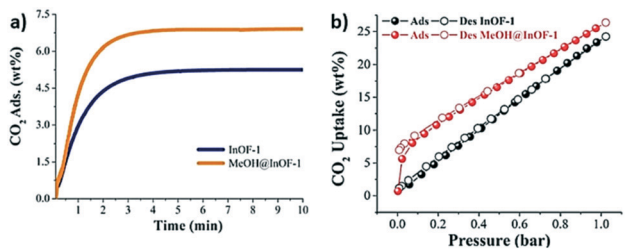


Fig. 3 Kinetic $CO_2$ uptake experiments performed at 303 K with a $CO_2$ flow of 60 mL $min^{-1}$ for InOF-1 (blue curve) and MeOH@MFM-300(In) (orange curve) (a) static $CO_2$ adsorption–desorption performed from 0 to 1 bar at 196 K on InOF-1 (black circles) and MeOH@MFM-300(In) (red circles) (b) (reproduced from ref. 48 with permission from The Royal Society of Chemistry).

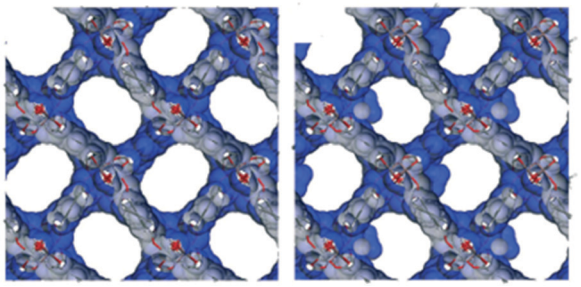

Fig. 4 van der Waals surface areas plotted for the DFT-optimized empty MFM-300(In) (right) and MeOH@MFM-300(In) (left) structures (reproduced from ref. 48 with permission from The Royal Society of Chemistry).

bottleneck effect (*vide supra*), which led to the enhancement in the adsorption of $CO_2$. More in-depth analysis of the hydrogen bonding between MeOH, $CO_2$ molecules and μ-OH bridging groups and their fundamental role in increasing the $CO_2$ uptake were detailed in a recent study.[54] Along with density functional theory (DFT), periodic calculations, and experimental *in situ* DRIFTS, the authors postulated four feasible mechanisms of $CO_2$ uptake in MFM-300(In) with MeOH pre-confined in its pores. According to the structure stability, the mechanisms are stated in the following order: (I) $CO_2$ and MeOH molecules interact with different $\mu_2$-OH bridging groups of MFM-300(In), and they could not interact with each other; (II) $CO_2$ interacts with MeOH; (III) $CO_2$ is trapped by MeOH due to the weak CH···O interactions and van der Waals interactions with MFM-300(In) and (IV) a $CO_2$ molecule replaces a MeOH molecule and forms a hydrogen bond with $\mu_2$-OH of InOF-1. This mechanism emphasises the importance of inorganic building units ($\mu_x$-OH) which are part of other metal clusters.[55]

Encouraged by the results, more recent studies explored the effect of confining 1-propanol[49] and 2-propanol[50] inside MFM-30O(In). Interestingly, dynamic and static experimental $CO_2$ isotherms showed that the confinement of a small amount of 1-propanol (2 wt%) did not improve the $CO_2$ adsorption capacity.[49] Grand canonical Monte Carlo (GCMC) simulations were carried out in order to understand this behavior. It was found that 1-propanol mixed with $CO_2$ tends to form clusters, instead of a localised distribution, causing blockage within the channels of MFM-300(In) and thus, a decrease of the $CO_2$ uptake. A study of 2-propanol[50] confinement in MFM-300(In) was recently reported in 2019. Dynamic experimental $CO_2$ isotherms were collected with 2.05 wt% 2-propanol, and a 1.25-fold increase of the $CO_2$ uptake (from 1.18 mmol $g^{-1}$ to 1.48 mmol $g^{-1}$) was observed. After 10 cycles of sorption–desorption, there was a slight reduction of the $CO_2$ capacity uptake (0.4 wt%). To gain a deeper understanding of this $CO_2$ capacity enhancement, quantum chemical models were calculated, demonstrating that this is a result of hydrogen bond interactions (2-PrOH with $\mu_2$-OH bridging groups, and 2-PrOH with $CO_2$) and the reduction of the pore volume generated by the presence of

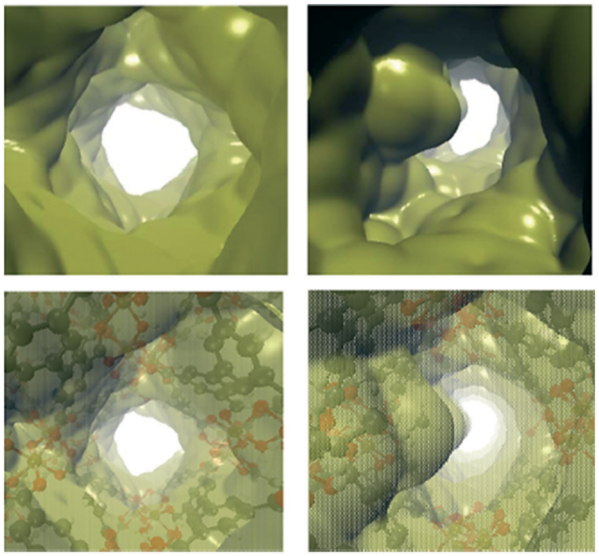

Fig. 5 Solid (top) and transparent (bottom) isosurface of the electron density ($\rho$ = 0.0003 a. u.), denoting the voids of the empty MFM-300(In) (left) and i-PrOH@MFM-300(In) (right) (reproduced from ref. 50 with permission from The Royal Society of Chemistry).

confined 2-propanol, which causes the bottleneck effect previously discussed (Fig. 5).

Confinement of ethanol within HKUST-1 (ref. 51) was also investigated. This study is relevant because the structure is different from MFM-300(In). HKUST-1 is not a hydroxo-functionalized material and it shows a rigid structure and open metal sites. HKUST is formed by square $Cu_2$ paddlewheel clusters linked by BTC ligands. This material has two pore size dimensions, a large one with around 10 and 11 Å and a second one with a diameter of 4 Å. For the $CO_2$ dynamic isotherm, a sample with a small amount of EtOH (3 wt%) confined in HKUST-1 pores was used and a slight adsorption capacity enhancement was observed (from 2.93 mmol $g^{-1}$ to 2.97 mmol $g^{-1}$) (Fig. 6a). It is worth noting that after 10 cycles of sorption–desorption, the crystal structure was retained, and the $CO_2$ capacity was maintained without the need for gas purging or thermal re-activation (Fig. 6b). A different behavior was observed when small quantities of water (3 wt%) were confined in the MOF, showing a decrease of $CO_2$ capacity uptake (Fig. 6a).

The effect on the $CO_2$ adsorption capacities when alcohol molecules (MeOH and 2-PrOH) were confined in MIL-53(Al) was also studied.[52] MIL-53(Al) is a flexible material formed by $\mu_2$-OH bridging groups in *trans* orientation. As Fig. 7a depicts, dynamic isotherms revealed a $CO_2$ adsorption enhancement when a small amount of MeOH and 2-propanol (2 wt%) was confined in MIL-53(Al) (1.07 mmol $g^{-1}$ and 1.022 mmol $g^{-1}$, respectively), in comparison to the fully activated material (0.79 mmol $g^{-1}$) (Fig. 7a). The static isotherm also showed a $CO_2$ capture enhancement when MeOH was confined (from 7.2 to 9.0 mmol $g^{-1}$) (Fig. 7b). The sorption–desorption process of MIL-53(Al), with MeOH confined showed a small loss of the $CO_2$ adsorption capacity (6.3% wt) after 10 cycles (Fig. 7c). Remarkably, this process only needed mild reactivation conditions. In addition, a structural model was optimised to visualise the hydrogen bonds expected between MeOH and the hydroxo functional groups of this MOF material. A minimal variation of the hydrogen bond length between $CO_2$–MeOH (1.79 Å) and $CO_2$–2-PrOH (1.85 Å) was found, and indeed this fact can explain the small difference in the $CO_2$ adsorption obtained between both confined molecules (Fig. 8).

In 2018, a study on the $CO_2$ adsorption properties (EtOH confined) of an Al(III)-based MOF material labeled MIL-53(Al)-TDC[34] was performed. MIL-53(AL)-TDC is a microporous material, constructed with 2,5-thiophenedicarboxylate (TDC) and Al(III), which provides a rigid structure. Kinetic $CO_2$ experimental isotherms were obtained with small amounts of EtOH confined. Interestingly, the $CO_2$ capture was not enhanced. An optimised model was calculated to visualize relevant hydrogen bonds, revealing that the position of the

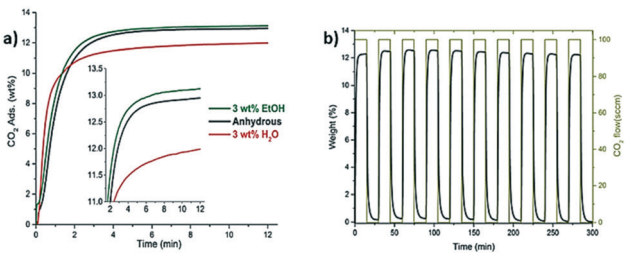


Fig. 6 $CO_2$ uptake experiments performed on HKUST-1 with small loadings of pre-adsorbed water and ethanol at 303 K (a). Inset: Zoom of $CO_2$ adsorption emphasising the slightly enhanced $CO_2$ capture with the use of ethanol. $CO_2$ cycling measurements for the ethanol impregnated HKUS-1 sample at 303 K, showing the reversibility of the capture process (b) (reproduced from ref. 51 with permission from The Royal Society of Chemistry).

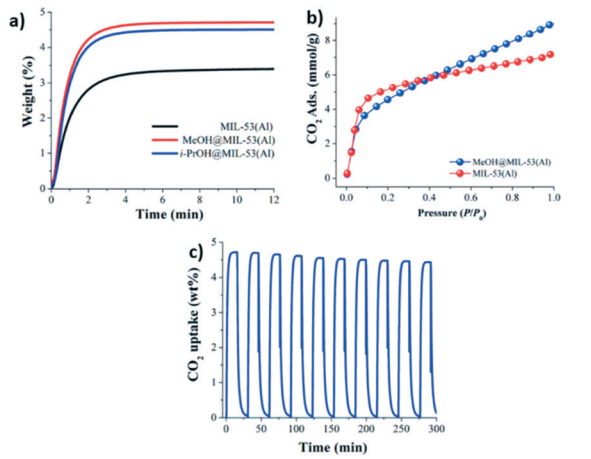


Fig. 7 Kinetic $CO_2$ uptake experiments at 30 °C with a $CO_2$ flow of 60 mL $min^{-1}$ in MIL-53(Al) (black curve); MeOH@MIL-53(Al) (red curve) and i-PrOH@MIL-53(Al) (blue curve) (a). Static $CO_2$ adsorption from 0 to 1 bar at 196 K on MIL-53(Al) (red circles) and MeOH@MIL-53(Al) (blue circles) (b). Adsorption–desorption cycling for MeOH@MIL-53(Al) (c) (reproduced from ref. 52 with permission from The Royal Society of Chemistry).

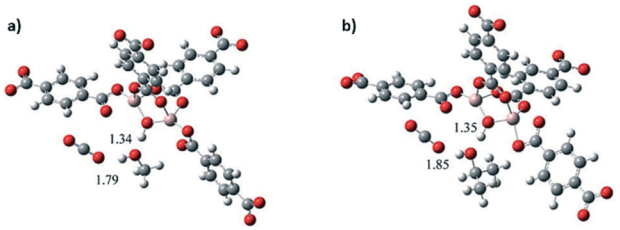


Fig. 8 Optimised structures of MIL-53(Al): (a) proposed model interacting with MeOH and $CO_2$ and (b) proposed model interacting with i-PrOH and $CO_2$ (reproduced from ref. 52 with permission from The Royal Society of Chemistry).

interaction between EtOH and $CO_2$ (EtOH···O═C═O) was out of plane, in other words, these molecules were not well-positioned for a favorable interaction and, therefore, $CO_2$ capture enhancement.

A new method was reported by Chen *et al.*[56] in 2018. Using a slurry mixture of ZIF-8/mIm (methylimidazole)–glycol for the capture of $CO_2$, *via* a hybrid absorption–adsorption method, they found that 5 w% mIm in the liquid phase increases the $CO_2$ capture in the presence of water.

On the other hand, the use of aminated solvents has been shown to be an interesting alternative for $CO_2$ capture. In this regard, a widely used technique is the introduction of alkyldiamine molecules inside MOF channels. Several studies have reported the increase of the $CO_2$ adsorption capacity by open metal sites (OMSs) and the generation of amine adsorption sites.[57–63] Herein, one amine group is coordinated to an open metal site, while the other one remains free to interact with $CO_2$ molecules, taking advantage of the affinity of basic amines with $CO_2$ molecules. However, this method requires the use of only MOFs with OMSs, which greatly hinders the recovery of $CO_2$ adsorbed. Similar to the diamine use mentioned above, another $CO_2$ adsorption approach has been investigated by observing the influence of alkylamine fixation in MOF materials with Brønsted acid–base pendent groups (such as UiO-66-$NH_2$ and Cr-MIL-101-$SO_3H$).[64] In this study, a noticeable increase in the $CO_2$ adsorption properties was observed and in the case of EDA-UiO-66 (EDA = ethylenediamine), a remarkable cyclability performance was shown. Nevertheless, in all adsorption experiments, the formation of carbamate as a by-product was detected.

Otherwise, amide molecules, *e.g. N*,*N*-dimethylformamide (DMF), *N*,*N*-diethylformamide (DEF), *N*,*N*-dimethylacetamide (DMA) and *N*-methyl-2-pyrrolidone (NMP), have shown a great influence on the physical and chemical properties of some MOFs.[65] In this context, Garcia-Garibay and co-workers[66] investigated the diffusion-controlled rotation of a triptycene-based MOF in a viscous environment induced by confined DMF. Accordingly, Lu and Usman[67] demonstrated how the DMF loading increased the dielectric constant in three isostructural 1D-MOFs based on Sr(II).

Motivated by the preliminary investigations on the use of amides in MOF materials, our group performed, in 2017 (ref. 68), the pre-confinement of DMF within MFM-300(In) to study the $CO_2$ adsorption properties. An enhancement in the $CO_2$ uptake was observed when MFM-300(In) was loaded with a minimal quantity of DMF (4.2 wt%). Dynamic and static $CO_2$ isotherms showed a 1.5-fold (1.83 mmol $g^{-1}$) and 1.4-fold (7.5 mmol $g^{-1}$) increase of the $CO_2$ captures, respectively (Fig. 9a and b), in comparison to dry adsorption measurements (1.19 mmol $g^{-1}$ and 5.5 mmol $g^{-1}$, respectively). Adsorption–desorption measurements revealed the stability of $CO_2$ adsorption even after 10 cycles under mild conditions (Fig. 9c). To provide evidence of host–guest hydrogen bonds, which are likely responsible for the increase of $CO_2$ adsorption, the single crystal X-ray diffraction structure of MFM-300(In) with DMF confined was determined. It was corroborated that DMF molecules were situated in an ideal position in a "dent in the wall" between the ligands. The angle formed is 115°, close to the theoretical

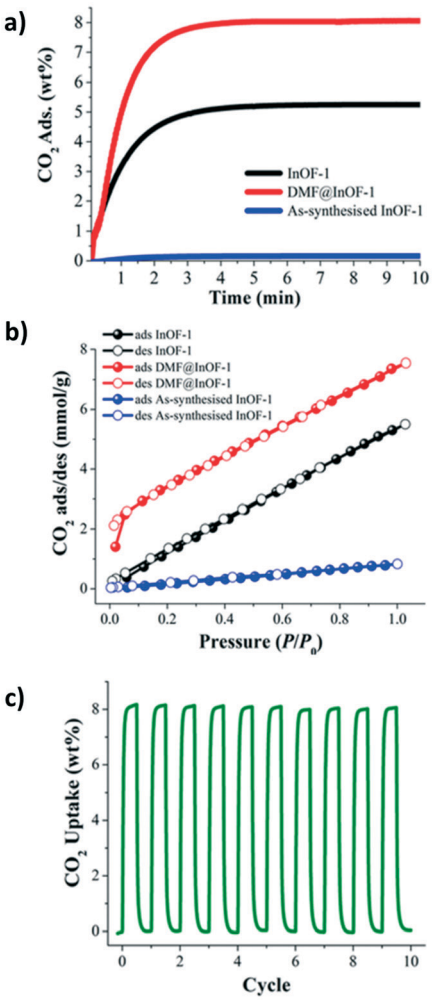


Fig. 9 (a) Kinetic $CO_2$ uptake experiments at 303 K on InOF-1, DMF@InOF-1, and as-synthesised InOF-1 (black, red, and blue lines respectively). (b) Static $CO_2$ adsorption/desorption at 1 bar and 196 K on InOF-1, DMF@InOF-1, and as-synthesized InOF-1 (black, red, and blue circles respectively). (c) Adsorption/desorption cycling for DMF@InOF-1. Reprinted with permission from ref. 68 (copyright 2017, American Chemical Society).

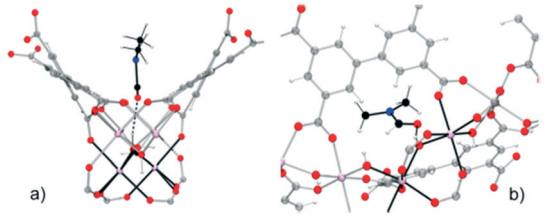


Fig. 10 Mutual orientations of the DMF molecules and the MFM-300(In) framework, showing the hydrogen bonds between the DMF and $In_2(\mu\text{-OH})$ groups (a) in the direction of the channel and (b) showing details of the hydrogen bonds. Reprinted with permission from ref. 68 (copyright 2017, American Chemical Society).

120° from $sp^2$ hybridization, and O–H···O is nearly linear (Fig. 10).

## 4. Confinement of aromatic and other molecules to enhance $CO_2$ capture

Up to this point, we have only considered the influence of small polar molecules (water, alcohols and amines) on the $CO_2$ uptake and how these pre-confined guest molecules interact simultaneously with the pore wall and the $CO_2$ molecule, mainly by hydrogen bonding and other weak interactions leading to micro-pockets and bottleneck behaviours.[29,47,68] It is worth mentioning that not only these types of pre-confinement molecules can enhance the $CO_2$ capture performance, but also recent investigations have shown how non-polar molecules such as toluene,[69] benzene[70] and other slightly bigger molecules (ionic liquids and dyes),[71] and even corrosive gases such as $SO_2$ can improve $CO_2$ capture[72] *via* reduction of the cross-sectional surface area and pore volume leading to a better packing of $CO_2$ molecules into MOF channels.

Following the same methodology, a small amount of toluene (1.5 wt%) was confined in MFM-300(In).[69] Interestingly, a 1.38-fold increase of $CO_2$ capture was obtained in contrast to the fully activated material under kinetic conditions (from 1.19 mmol $g^{-1}$ to 1.65 mmol $g^{-1}$) (Fig. 11a). When 6 cycles of adsorption–desorption were achieved, the $CO_2$ adsorption capacity was not affected (Fig. 11b), and its crystallinity did not suffer from any change. The isosteric heat of adsorption ($\Delta H_{ads}$ = −46.81 kJ $mol^{-1}$), experimentally evaluated, suggests the substantial affinity of MFM-300(In) toward toluene. Theoretical studies and DRIFTS experiments were carried out to investigate the predominant interactions in the adsorption process. DFT studies revealed π–π stacking interactions between the toluene molecule and the aromatic rings of the MFM-300(In) linkers. This was corroborated by electron density analysis, wherein weaker interactions were observed, such as C–H···O hydrogen bonds and C···C, and no typical H···H interactions were even found.[73] The $CO_2$ capture enhancement of toluene@MFM-300(In) was attributed to the bottleneck effect, and the interactions between toluene···$CO_2$ and MFM-300(In) ···$CO_2$.[47] The electron density isosurface showed a toluene molecule per unit cell confined in MFM-300(In), generating a reduction of 15% of the pore dimensions compared with the pristine material (Fig. 12). Moreover, an optimised model (Fig. 13) showed how the $CO_2$ molecule interacts with the centroids of aromatic rings of toluene and MFM-300(In) linkers, contributing to the $CO_2$ capture.

In addition, MFM-300(In) was pre-loaded with benzene to have a direct comparison. Thus, a small amount of benzene (1.5 wt%) was pre-confined and the $CO_2$ adsorption was evaluated,[65] resulting in a 1.6-fold increase under dynamic conditions (Fig. 14a). Fig. 14b shows eight $CO_2$ adsorption–desorption cycles on benzene@MFM-300(In) with an outstanding $CO_2$ reversibility performance. The isosteric heat of adsorption ($\Delta H_{ads}$ = −25.1 kJ $mol^{-1}$) suggested a weaker interaction between benzene and the MOF material in comparison to that with toluene.[69] According to computational studies, π···π interactions, weak C–H···O hydrogen bonds, and medium strength C–H···H–O hydrogen bonds were found by confining benzene in MFM-300(In), as previously stated by confining toluene.[64] The optimized structures depicted in Fig. 15 show the most stable arrangement of $CO_2$ molecules inside the channels of the MOF material. Therefore, the $CO_2$ molecule can be found (i) interacting with the $\mu_2$-OH bridge group and with the centroid of the aromatic ring in the linker, and (ii) parallel to the aromatic ring of the linker.

In this context, the confinement of ionic liquids (ILs) within MOFs to enhance the $CO_2$ adsorption has also recently

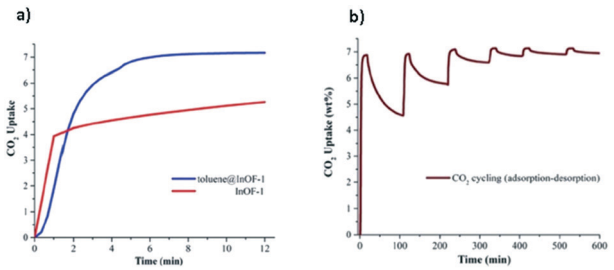


Fig. 11 $CO_2$ dynamic adsorption experiments performed at 298 K for InOF-1 (red curve) and toluene@InOF-1 (blue curve) (a). Adsorption–desorption $CO_2$ cycling for toluene@InOF-1 (b) (reproduced from ref. 69 with permission from The Royal Society of Chemistry).

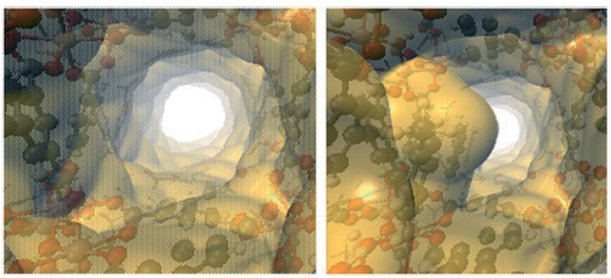

Fig. 12 Electron density isosurfaces, denoting the void channels of the pristine (left) and toluene-functionalized MFM-300(In) (right) (reproduced from ref. 69 with permission from The Royal Society of Chemistry).

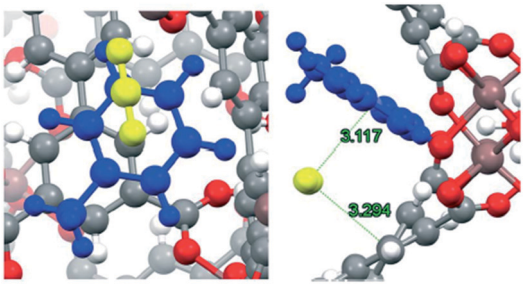


Fig. 13 Close up (left) and pore channel (right) views of $CO_2$ captured by toluene-functionalized InOF-1. Toluene, $CO_2$, and the MFM-300 framework are depicted in blue, yellow and gray, respectively. Reproduced from ref. 69 with permission from The Royal Society of Chemistry.

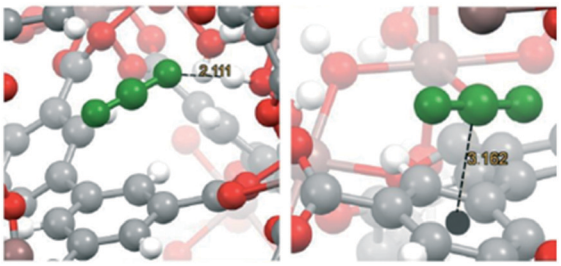


Fig. 15 Two possible interactions between a $CO_2$ molecule and the MFM-300(In) material: $\mu_2$-OH···O=C=C interaction (left) and $CO_2$···MFM-300(In) linker centroid (right). The $CO_2$ molecule is depicted in green color. The aromatic ring mass centre is indicated with a black sphere (reproduced from ref. 70 with permission from The Royal Society of Chemistry).

been investigated. In 2015, Yang and Ban[71a] used ZIF-8 nanocages, a material with limited $CO_2$ capture performance, to introduce an imidazolium-based IL [bmim][$Tf_2N$] by ionothermal synthesis (Fig. 16). The authors chose this IL because the $Tf_2N$ mono-anionic species has been shown to have a remarkable affinity for the $CO_2$ molecule and its cationic counterpart (bmim) fits properly into the ZIF-8 microporous cavity. A reduction of the pore volume and surface area was observed. Despite these changes, the $CO_2$ capture (particularly in the low-pressure range) was almost two-fold enhanced (from 0.28 mmol $g^{-1}$ to 0.45 approximately at 0.3 bar and 298 K) with a molar ratio of 0.235 IL/ZIF-8. In addition, this improvement is due to two contributions: (i) the reduction of the pore dimensions of ZIF-8 and (ii) the ion-induced dipole interactions between the IL and the $CO_2$ molecules, but more details are needed to confirm such a hypothesis. Although the confinement of ILs into ZIF-8 was not shown to be the best alternative to improve the $CO_2$ capture compared with other pre-confined molecules (water, alcohols and amines), the use of larger molecules as ILs proves that the reduction of a cross section of pore volume or the formation of micropockets[29] can be induced in different MOFs to modify their gas adsorption properties.

Similarly, Wu and co-workers[71b] confined dye molecules, such as cationic rhodamine B, anionic CR, and neutral melanin, which are aromatic molecules with different functional groups (–OH and –NH). The confinement of these dye molecules within a mesoporous MOF material, labeled CZJ-10, was performed in different quantities (0.28, 0.04, and 13.1 mol per unit of material, respectively). CZJ-10 is assembled from 4,4′,4″-benzene-1,3,5-triyltricinnamic acid as a linker and $Cu_2(CO_2)$ paddlewheels as the inorganic building unit. Unlike other materials with open metal sites that have been used in the small polar solvent pre-loading approach (*e.g.*, water and alcohols within HKUST),[38,51] the CZJ-10 pre-loaded with each dye molecule (RB@CZJ-10, CR@CZJ-10 and melanin@CZJ-10, respectively) showed a significant improvement of $CO_2$ capture (Fig. 17). Melanin@CZJ-10 achieved slightly the best $CO_2$ uptake compared to the other dye@CZJ-10 (1.46, 1.37 and 1.63 mmol $g^{-1}$ for RB@CZJ-10, CR@CZJ-10 and melanin@CZJ-10, respectively), and an almost 2.5-fold increase compared to pristine CZJ-10 (0.67 mmol $g^{-1}$) at 1 bar and 298 K. The authors attributed this enhancement to the addition of new binding sites inside the pores, resulting in a stronger affinity to $CO_2$ molecules. To support this statement, the authors encapsulated triphenylmethane (TPM), a neutral aromatic molecule, into

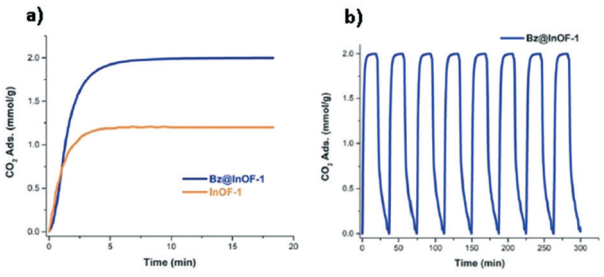


Fig. 14 $CO_2$ uptake experiments performed in InOF-1 (orange curve) and Bz@InOF-1 (blue curve) at 298 K (a). $CO_2$ cycling measurements for Bz@InOF-1 at 298 K (b) (reproduced from ref. 70 with permission from The Royal Society of Chemistry).

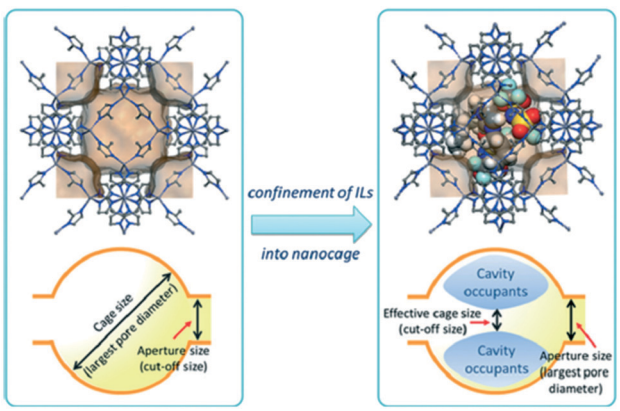


Fig. 16 Illustration of the cavity-occupying concept for tailoring the molecular sieving properties of ZIF-8 by incorporation of RTILs. The cut-off size shifts from the aperture size of the six-membered ring to the reduced effective cage size by confinement of [bmim][$Tf_2N$] in a ZIF-8 cage. Reprinted with permission from ref. 71*a* (copyright 2015, Wiley-VCH Verlag GmbH & Co.).

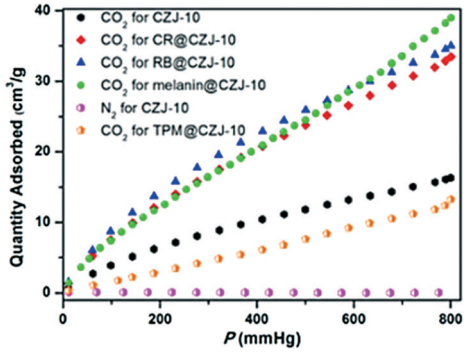


**Fig. 17** $CO_2$ adsorption isotherms of CZJ-10, RB@CZJ-10, CR@ CZJ-10, melanin@CZJ-10, and TPM@CZJ-10, and $N_2$ adsorption isotherm of CZJ-10 at 298 K. Reprinted with permission from ref. 71*b* (copyright 2017, American Chemical Society).

CZJ-10 (TPM@CZJ-10). The $CO_2$ isotherm of TPM@CZJ-10 measured up to 1 bar and 298 K reached only 0.55 mmol $g^{-1}$, resulting in a lower $CO_2$ uptake compared to pristine CJZ-10.

On the other hand, the gas co-adsorption process in traditional porous materials has been suggested as an excellent alternative to improve the adsorption of toxic gases by either host–guest or guest–guest interactions.[74] In this context, Son and Chihaia highlighted the fundamental role of computational research using a predictive tool in the improvement of $CO_2$ capture.[72] They evaluated the simultaneous adsorption of $CO_2$ and $SO_2$ in a Ni-based MOF ($Ni(bdc)(ted)_{0.5}$) by DFT studies (Fig. 18). The authors observed that the material exhibited a higher affinity to $SO_2$ over $CO_2$. Additionally, the $CO_2$ molecule can interact with the $SO_2$ molecule by weak interaction between the oxygen atom of $CO_2$ and the sulphur of $SO_2$ ($CO_2\cdots SO_2$) (Fig. 18b). This example suggests that the co-adsorption method can be one of the best alternatives to improve the $CO_2$ gas adsorption in MOFs especially at the industrial level, since not only the $SO_2$ molecule can be a good candidate, but also molecules with a relevant polar nature (*e.g.*, $NH_3$ and $H_2S$ which are present in some flue gas streams) can be used for this task.

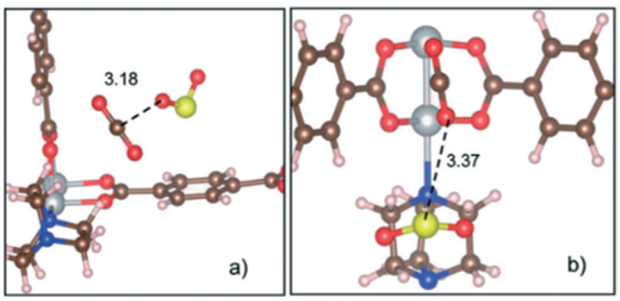


**Fig. 18** Two main configurations for co-adsorption of $SO_2$ and $CO_2$ molecules in the $Ni(bdc)(ted)_{0.5}$ material. (a) Less stable configuration with an $SO_2\cdots CO_2$ interaction type and a binding energy of −0.33 eV. (b) Most stable configuration with a $CO_2\cdots SO_2$ interaction type and a binding energy of −0.65 eV and a length of 3.37 Å. C (brown), O (red), H (white), S (yellow), N (blue), and Ni (silver) (reproduced from ref. 72 with permission from The Royal Society of Chemistry).

## 5. Conclusions and outlook

Concern behind designing better materials for environment harmful gases uptake, *e.g.* $CO_2$, is growing. MOFs have been widely studied for this aim, due to the ease of modulating the chemical and physical environments of their pores, and therefore, the way they interact with $CO_2$ molecules. In the recent years, a series of studies have reported the post-synthetic modification of MOFs by confining polar and non-polar molecules, achieving a significant improvement of $CO_2$ capture. Herein, we had cited the progress for this new strategy.

Water confinement has been studied in meso and microporous MOFs that contain hydroxo bridge groups ($\mu_x$-OH) in their pores, which form hydrogen bonds with water molecules. These host–guest interactions are responsible for the so-called bottleneck effect, which is defined as a reduction of the pore volume, not allowing the free passage of $CO_2$ flow, and as a result, $CO_2$ molecules can be accommodated more effectively in the cavities.

These results encouraged the study of confining molecules with different polarities. A small quantity of molecules, such as EtOH, MeOH, 2-propanol and DMF (in the range of 2.0–4.2 wt%), were confined in hydroxo-functionalized MOFs ((MFM-300(In), MIL-53(Al) and MIL-53(Al)-TDC)) and a non-hydroxo-functionalized MOF (HKUST-1), showing an improvement of the $CO_2$ capture. Hydrogen bonds between the polar molecules and the hydroxo bridge groups were demonstrated by computational studies. According to these results, the best enhancement was achieved with a 2.7-fold increase with the confinement of EtOH in MFM-300(In). Interestingly, an enhancement of $CO_2$ capture was also found when non-polar molecules, such as toluene and benzene, were confined in the pores. Computational studies suggest that $\pi\cdots\pi$ stacking-type interactions, weak C–H$\cdots$O hydrogen bonds, and medium strength C–H$\cdots$H–O are responsible for the stronger interaction with $CO_2$ molecules and the bottleneck effect.

Similarly, ILs were confined in the nanocages of ZIF-8 and the $CO_2$ capture was also improved, despite a reduction of the pore volume being observed; the $CO_2$ adsorption mechanism is not well-known. Furthermore, aromatic dye molecules confined in CZJ-10 also improved the $CO_2$ capture because of the additional binding sites provided by the confined molecules.

Clearly, this new strategy of introducing molecules into MOF pores does not only significantly enhance the $CO_2$ adsorption but also avoid the negative effect of water and other solvents in capturing $CO_2$, enabling more real applications of MOFs in industry. Even though significant progress has been made in the last five years, some challenges lie ahead. For example, changing the chemical environment or the topology of the pores by functionalizing

 

MOFs with other functional groups or introducing molecules with a different kinetic diameter or polarity. All these studies could provide a clear understanding of the $CO_2$ adsorption mechanism.

In addition, the early post-modification approach has been shown to have some relevant advantageous/disadvantageous points. For example, the use of any pre-confined molecule (*vide supra*) represents a more suitable and cheaper strategy to improve the $CO_2$ capture in MOFs than other pre- or post-modifications (*i.e.*, the insertion of polar functional groups or the generation of OMSs), due to the easy adaptation of molecules into the cavities of MOFs and the low cost of organic/inorganic molecules (water, alcohols and amines). Furthermore, as far as we have investigated, the pre-confinement of alcohols can be considered the best option to improve the $CO_2$ capture with an industrial profile, mainly due to three reasons: (i) relevant improvement of $CO_2$ gas adsorption, especially at a low pressure range; (ii) low pre-confined amount of alcohol needed to achieve $CO_2$ enhancement; and (iii) good recyclability, since this type of molecule has been shown to be present in at least ten $CO_2$ adsorption–desorption cycles. However, a clear disadvantage of this methodology is the nature of the molecule to be used, *e.g.*, the nature of water confinement requires the use of MOFs with a high structural stability to water (to avoid structural collapse) and a remarkable hydrophilic character to retain $H_2O$ into the cavities. Other concerns regarding this methodology are that the confined molecules should not exceed the minimum range to achieve such improvement (between 1 to 5 wt%, in most cases), and the toxicity of aromatic molecules such as benzene and toluene.

## Conflicts of interest

There are no conflicts to declare.

## Acknowledgements

The authors thanks PAPIIT UNAM (IN202820), México for financial support. We thank U. Winnberg (ITAM) and E. Martínez-Ahumada (IIM-UNAM) for scientific discussions and G. Ibarra-Winnberg for scientific encouragement.

## Notes and references

1 K. Anderson and A. Bows, *Philos. Trans. R. Soc., A*, 2011, **369**, 20–44.
2 N. Watts, M. Amann, N. Arnell, S. Ayeb-Karlsson and H. Montgomery, *Lancet*, 2019, **394**, 1836–1879.
3 B. R. Villanueva, M. B. Salvador and R. G. Huelgas, *Rev. Clin. Esp.*, 2019, **219**, 260–265.
4 G. Astarita, *Ind. Eng. Chem. Fundam.*, 1963, **2**(4), 294–297.
5 A. El-Sayed and M. Kamel, *Environ. Sci. Pollut. Res.*, 2020, 1–17.
6 U. S. Environmental Protection Agency, *Inventory of U.S. Greenhouse Gas Emissions and Sinks*, 2018, https://www.epa.gov/ghgemissions/inventory-us-greenhouse-gas-emissions-and-sinks.
7 (*a*) B. Aghel, S. Sahraie, E. Heidaryan and K. Varmira, *Process Saf. Environ. Prot.*, 2019, **131**, 152–159; (*b*) M. J. Kim, S. W. Choi, H. Kim, S. Mun and K. B. Lee, *Chem. Eng. J.*, 2020, **397**, 125404; (*c*) S. T. Hosseini, H. Raissi and M. Pakdel, *New J. Chem.*, 2020, **44**, 7771–7779; (*d*) M. Younas, M. Sahail, L. K. Leong, M. J. K. Bashir and S. Sumathi, *Int. J. Environ. Sci. Technol.*, 2016, **13**, 1839–1860.
8 J. J. Chai, T. C. Johnstone, D. Voicu, P. Mehlman, F. Dielmann, E. Kumacheva and D. W. Stephan, *Chem. Sci.*, 2017, **8**, 3270–3275.
9 K. Sumida, D. L. Rogow, J. A. Mason, T. M. McDonald, E. D. Bloch, Z. R. Herm, T.-H. Bae and J. R. Long, *Chem. Rev.*, 2012, **112**, 724–781.
10 G. Singh, J. Lee, A. Karakoti, R. Bahadur and J. Yi, *Chem. Soc. Rev.*, 2020, **49**, 4360–4404.
11 (*a*) G. T. Rochelle, *Science*, 2009, **325**, 1652–1654; (*b*) R. V. Siriwardane, M.-S. Shen, E. P. Fisher and J. Losch, *Energy Fuels*, 2005, **19**(3), 1153–1159; (*c*) S. Dinda, P. Murge and C. Paruchuri, *Bull. Mater. Sci.*, 2019, **42**, 1–9.
12 (*a*) S.-H. Hong, M.-S. Jang, S. J. Cho and W.-S. Ahn, *Chem. Commun.*, 2014, **50**, 4927–4930; (*b*) F. Su and C. Lu, *Energy Environ. Sci.*, 2012, **5**, 9021–9027.
13 (*a*) C. M. Mfoumou, S. Mignard and T. Belin, *Adsorpt. Sci. Technol.*, 2018, **36**, 1246–1259; (*b*) G. Li, P. Xiao, P. A. Webley, J. Zhang and R. Singh, *Energy Procedia*, 2009, **1**, 1123–1130.
14 M. Ding, R. W. Flaig, H.-L. Jiang and O. M. Yaghi, *Chem. Soc. Rev.*, 2019, **48**, 2783–2828.
15 (*a*) Z. Hu, Y. Wang, B. B. Shah and D. Zhao, *Adv. Sustainable Syst.*, 2019, **3**, 1800080; (*b*) J.-R. Li, R. J. Kuppler and H.-C. Zhou, *Chem. Soc. Rev.*, 2009, **38**, 1477–1504; (*c*) J.-R. Li, J. Sculley and H.-C. Zhou, *Chem. Rev.*, 2012, **112**(2), 869–932.
16 S. Keskin, T. M. Van Heest and D. S. Sholl, *ChemSusChem*, 2010, **3**, 879–891.
17 P. M. Schoenecker, C. G. Carson, H. Jasuja, C. J. J. Flemming and K. S. Walton, *Ind. Eng. Chem. Res.*, 2012, **51**, 6513–6519.
18 Y. Xiong, Y. Gao, X. Guo, Y. Wang, X. Su and X. Sun, *ACS Sustainable Chem. Eng.*, 2019, **7**, 3120–3126.
19 D. Banerjee, B. J. Deibert and H. W. J. Li, *Encycl. Inorg. Bioinorg. Chem.*, 2014, **1**, 1–21.
20 Y. Belmabkhout, V. Guillerm and M. Eddaoudi, *Chem. Eng. J.*, 2016, **296**, 386–397.
21 C. G. Piscopo and S. Loebbecke, *ChemPlusChem*, 2020, **85**, 538–547.
22 (*a*) Z. Zhang, Z.-Z. Yao, S. Xiang and B. Chen, *Energy Environ. Sci.*, 2014, **7**, 2868–2899; (*b*) J.-R. Li, Y. Ma, M. C. McCarthy, J. Sculley, J. Yu, H.-K. Jeong, P. B. Balbuena and H.-C. Zho, *Coord. Chem. Rev.*, 2011, **255**, 1791–1823.
23 X. Si, C. Jiao, F. Li, J. Zhang, S. Wang, S. Liu, Z. Li, L. Sun, F. Xu, Z. Gabelicad and C. Schick, *Energy Environ. Sci.*, 2011, **4**, 4522–4527.
24 (*a*) M. P. Suh, H. J. Park, T. K. Prasad and D.-W. Lim, *Chem. Rev.*, 2012, **112**, 782–835; (*b*) Y. Harada, Y. Hijikata, S. Kusaka, A. Hori, Y. Ma and R. Matsuda, *Dalton Trans.*,

2019, **48**, 2545–2548; (*c*) J. N. Hall and P. Bollini, *React. Chem. Eng.*, 2019, **4**, 207–222.
25 E. González-Zamora and I. A. Ibarra, *Mater. Chem. Front.*, 2017, **1**, 1471–1484.
26 (*a*) C. Wang, X. Liu, N. K. Demir, J. P. Chen and K. Li, *Chem. Soc. Rev.*, 2016, **45**, 5107–5134; (*b*) N. C. Burtch, H. Jasuja and K. S. Walton, *Chem. Rev.*, 2014, **114**, 10575–10612.
27 (*a*) W. Li, X. Xia, M. Cao and S. Li, *J. Mater. Chem. A*, 2019, **7**, 7470–7479; (*b*) M. F. Lange, B. L. Velzen, C. P. Ottevanger, K. J. F. M. Verouden, L.-C. Lin, T. J. H. Vlugt, J. Gascon and F. Kaptein, *Langmuir*, 2015, **31**, 12783–12796; (*c*) Y. I. Aristov, *J. Chem. Eng. Jpn.*, 2007, **40**, 1242–1251.
28 A. O. Yazaydın, A. I. Benin, S. A. Faheem, P. Jakubczak, J. J. Low, R. R. Willis and R. Q. Snurr, *Chem. Mater.*, 2009, **21**, 1425–1430.
29 E. Soubeyrand-Lenoir, C. Vagner, J. W. Yoon, P. Bazin, F. Ragon, Y. K. Hwang, C. Serre, J.-S. Chang and P. L. Llewellyn, *J. Am. Chem. Soc.*, 2012, **134**, 10174–10181.
30 R. A. Peralta, B. Alcántar-Vázquez, M. Sánchez-Serratos, E. González-Zamora and I. A. Ibarra, *Inorg. Chem. Front.*, 2015, **2**, 898–903.
31 J. R. Álvarez, R. A. Peralta, J. Balmaseda, E. González-Zamora and I. A. Ibarra, *Inorg. Chem. Front.*, 2015, **2**, 1080–1084.
32 E. Sánchez-González, J. R. Álvarez, R. A. Peralta, A. Campos-Reales-Pineda, A. Tejeda-Cruz, E. Lima, J. Balmaseda, E. González-Zamora and I. A. Ibarra, *ACS Omega*, 2016, **1**, 305–310.
33 M. Sánchez-Serratos, P. A. Bayliss, R. A. Peralta, E. González-Zamora, E. Lima and I. A. Ibarra, *New J. Chem.*, 2016, **40**, 68–72.
34 G. A. González-Martínez, T. Jurado-Vázquez, D. Solís-Ibarra, B. Vargas, E. Sánchez-González, A. Martínez, R. Vargas, E. González-Zamora and I. A. Ibarra, *Dalton Trans.*, 2018, **47**, 9459–9465.
35 V. B. López-Cervantes, E. Sánchez-González, T. Jurado-Vázquez, A. Tejada-Cruz, E. González-Zamora and I. A. Ibarra, *Polyhedron*, 2018, **155**, 163–169.
36 M. Sagastuy-Breña, P. G. M. Mileo, E. Sánchez-González, J. E. Reynods III, T. Jurado-Vázquez, J. Balmaseda, E. González-Zamora, S. Devautour-Vinot, S. M. Humphrey, G. Maurin and I. A. Ibarra, *Dalton Trans.*, 2018, **47**, 15827–15834.
37 H. Furukawa, N. Ko, Y. B. Go, N. Aratani, S. B. Choj, E. Choi, A. Ö. Yazaydin, R. Q. Snurr, M. O'Keeffe, J. Kim and O. M. Yagui, *Science*, 2010, **329**, 424–428.
38 Y. Chen, Z. Quiao, J. Huang, H. Wu, J. Xiao, Q. Xia, H. Xi, J. Hu, J. Zhou and Z. Li, *ACS Appl. Mater. Interfaces*, 2018, **10**, 38638–38647.
39 J. Liu, Y. Wang, A. I. Benin, P. Jakubczak, R. R. Willis and M. D. Le Van, *Langmuir*, 2010, **26**, 14301–14307.
40 A. C. Kizzie, A. G. Wong-Foy and A. J. Matzger, *Langmuir*, 2011, **27**, 6368–6373.
41 P. Vervoorts, A. Schneemann, I. Hante, J. Pirillo, Y. Hijikata, T. Toyao, K. Kon, K.-I. Shimizu, T. Nakamura, S.-I. Noro and R. A. Fisher, *ACS Appl. Mater. Interfaces*, 2020, **12**(8), 9448–9456.
42 G. D. Pirngruberx, L. Hamon, S. Bourrelly, P. L. Llewelly, E. Lenoir, V. Guillerm, C. Serre and T. Devic, *ChemSusChem*, 2012, **5**, 762–776.
43 Q. Liu, L. Q. Ning, S. D. Zheng, M. N. Tao, Y. Shi and Y. He, *Sci. Rep.*, 2013, **3**, 1–6.
44 S.-I. Noro, R. Matsuda, Y. Hijikata, Y. Inubashi, S. Takeda, S. Kitagawa, Y. Takahashi, M. Yoshitake, K. Kubo and T. Nakamura, *ChemPlusChem*, 2015, **80**, 1517–1524.
45 Y. Liu, J. Liu, Y. S. Lin and M. Chang, *J. Phys. Chem. C*, 2014, **118**, 6744–6751.
46 D. Alvarado-Alvarado, J. H. González-Estefan, J. Gabriel-Flores, J. R. Álvarez, J. Aguilar-Pliego, A. Islas-Jácome, G. Chastanet, E. González-Zamora, H. A. Lara-García, B. Alcántar-Vázquez, M. Gonidec and I. A. Ibarra, *Organometallics*, 2020, **39**(7), 949–955.
47 R. A. Peralta, A. Campos-Reales-Pineda, H. Pfeiffer, J. R. Álvarez, J. A. Zárate, J. Balmaseda, E. González-Zamora, A. Martínez, D. Martínez-Ortero, V. Jancik and I. A. Ibarra, *Chem. Commun.*, 2016, **52**, 10273–10276.
48 E. Sánchez-González, P. G. M. Mileo, J. R. Álvarez, E. González-Zamora, G. Maurin and I. A. Ibarra, *Dalton Trans.*, 2017, **46**, 15208–15215.
49 J. R. Álvarez, P. G. M. Mileo, E. Sánchez-González, J. A. Zárate, J. Rodríguez-Hernández, E. González-Zamora, G. Maurin and I. A. Ibarra, *J. Phys. Chem. C*, 2018, **122**(10), 5566–5577.
50 J. E. Sánchez-Bautista, B. Landeros-Rivera, T. Jurado-Vázquez, A. Martínez, E. González-Zamora, J. Balmaseda, R. Vargas and I. A. Ibarra, *Dalton Trans.*, 2019, **48**, 5176–5182.
51 J. R. Álvarez, E. Sánchez-González, E. Pérez, E. Schneider-Revueltas, A. Martínez, A. Tejeda-Cruz, A. Islas-Jácome, E. González-Zamora and I. A. Ibarra, *Dalton Trans.*, 2017, **46**, 9192–9200.
52 J. A. González-Martínez, J. A. Zárate, A. Martínez, E. Sánchez-González, J. R. Álvarez, E. Lima, E. González-Zamora and I. A. Ibarra, *RSC Adv.*, 2017, **7**, 24833–24840.
53 E. Sánchez-González, J. G. Flores, J. C. Flores-Reyes, I. Morales-Salazar, R. E. Blanco-Carapia, M. A. Rincón-Guevara, A. Islas-Jácome, E. González-Zamora, J. Aguilar-Pliego and I. A. Ibarra, *Materials*, 2020, **13**, 1840.
54 H. A. Lara-García, B. Landeros-Rivera, E. González-Zamora, J. Aguilar-Pliego, A. Gómez-Cortés, A. Martínez, R. Vargas, G. Díaz and I. A. Ibarra, *Dalton Trans.*, 2019, **48**, 8611–8616.
55 P. V. D. Voort, K. Leus, Y.-Y. Liu, M. Vandichel, V. V. Speybrock, M. Waroquier and S. Biswas, *New J. Chem.*, 2014, **38**, 1853–1867.
56 C. Jia, H. Li, B. Liu, Z. Qiao, Z. Zhang, C. Sun, L. Yang and G. Chen, *Ind. Eng. Chem. Res.*, 2018, **57**(37), 12494–12501.
57 A. Demessence, D. M. D'Alessandro, M. Lin-Foo and J. R. Long, *J. Am. Chem. Soc.*, 2009, **131**(25), 8784–8786.
58 S. Choi, T. Watanabe, T. Bae, D. S. Sholi and C. W. Jones, *J. Phys. Chem. Lett.*, 2012, **3**, 1136–1141.
59 N. Wang, A. Mundstock, Y. Liu, A. Huang and J. Caro, *Chem. Eng. Sci.*, 2015, **124**, 27–36.
60 F. Martínez, R. Sanz, G. Orcajo, D. Briones and V. Yángüez, *Chem. Eng. Sci.*, 2016, **142**, 56–61.

 

61 X. Su, L. Bromberg, V. Martis, F. Simeon, A. Huq and T. A. Hatton, *ACS Appl. Mater. Interfaces*, 2017, **9**, 11299–11306.
62 N. Vrtovec, M. Mazaj, G. Buscarino, A. Terracina, S. Agnello, I. Arčon, J. Kovač and N. Z. Logar, *Cryst. Growth Des.*, 2020, **20**, 5455–5465.
63 V. Irani, A. Tavasoli, A. Maleki and M. Vahidi, *Int. J. Hydrogen Energy*, 2018, **43**, 5610–5619.
64 (*a*) H. Molavi, F. A. Joukani and A. Shojaei, *Ind. Eng. Chem. Res.*, 2018, **57**, 7030–7039; (*b*) H. Li, K. Wang, D. Feng, Y.-P. Chen, W. Verdeegal and H.-C. Zhou, *ChemSusChem*, 2016, **9**, 1–10.
65 (*a*) Z. Akimbekov, D. Wu, C. Brozek, M. Dinca and A. Navrotsky, *Phys. Chem. Chem. Phys.*, 2016, **18**, 1158–1162; (*b*) P. A. Konik, E. A. Berdonosova, I. M. Savvotin and S. N. Klyamkin, *Microporous Mesoporous Mater.*, 2019, **277**, 132–135.
66 X. Jiang, H.-B. Duan, S. I. Khan and M. A. Garcia-Garibay, *ACS Cent. Sci.*, 2016, **2**(9), 608–613.
67 M. Usman, P.-H. Feng, K.-R. Chiou, J.-W. Chen, L.-W. Lee, Y.-H. Liu and K.-L. Lu, *ACS Appl. Electron. Mater.*, 2019, **1**, 836–844.
68 E. Sánchez-González, E. González-Zamora, D. Martínez-Otero, V. Jancik and I. A. Ibarra, *Inorg. Chem.*, 2017, **56**(10), 5863–5872.
69 L. P. Garrido-Olvera, J. E. Sánchez-Bautista, D. Alvarado-Alvarado, B. Laderos-Rivera, J. Raziel-Álvarez, R. Vargas, E. González-Zamora, J. Balmaseda, H. A. Lara-García, A. Martínez and I. A. Ibarra, *RSC Adv.*, 2019, **9**, 32864–32872.
70 L. J. Barrios-Vargas, J. G. Ruíz-Montoya, B. Landeros-Rivera, J. Raziel-Álvarez, D. Alvarado-Alvarado, R. Vargas, A. Martínez, E. González-Zamora, L. M. Cáceres, J. C. Morales and I. A. Ibarra, *Dalton Trans.*, 2020, **49**, 2786–2793.
71 (*a*) Y. Ban, Z. Li, Y. Li, Y. Peng, H. Jian, W. Jiao, A. Guo, P. Wang, Q. Yang, C. Zhong and W. Yang, *Angew. Chem., Int. Ed.*, 2015, **54**, 15483–15487; (*b*) M. Zhao, S. Ou and C.-D. Wu, *Cryst. Growth Des.*, 2017, **17**, 2688–2693.
72 D. N. Son, T. T. T. Huong and V. Chihaia, *RSC Adv.*, 2018, **8**, 38648–38655.
73 (*a*) C. F. Matta, J. Hernández-Trujillo, T. H. Tang and R. F. Bader, *Chem. – Eur. J.*, 2003, **9**, 1940–1951; (*b*) J. D. Dunitz and A. Gavezzotti, *Angew. Chem., Int. Ed.*, 2005, **44**, 1766–1787.
74 K. V. Kumar and F. Rodríguez-Reinoso, *Nanotechnology*, 2012, **24**, 035401.